WOOD RESEARCH doi.org/10.37763/wr.1336-4561/66.6.955968
e-ISSN 2729-8906
66(6): 2021 955-968 pp.

RESEARCH ON SHEAR PERFORMANCE OF COMPONENTS CONNECTED BY BEECH AND SELF-TAPPING SCREW COMPOSITE DOWELS

XUDONG ZHU[1,2,3]
[1]NANJING FORESTRY UNIVERSITY
[2]YANGZHOU POLYTECHNIC INSTITUTE
[3]YANGZHOU UNIVERSITY
CHINA

YINGYING XUE, XUEWEN ZHANG, PENGFEI QI, JIE SHEN
YANGZHOU POLYTECHNIC INSTITUTE
CHINA

CHANGTONG MEI
NANJING FORESTRY UNIVERSITY
CHINA

(RECEIVED MARCH 2021)

ABSTRACT

This study examined the properties of components connected by beech and self-tapping screw composite dowels (group C). As a contrast, the components connected by beech dowels and self-tapping screws individually were tested. The test results indicated that the properties of the components connected by beech dowels (group B) were better than those connected by self-tapping screws (group S), except the ductility coefficient, final displacement, and energy consumption. On the other hand, the main failure modes of groups B and S were the broken beech dowel and the bent self-tapping screw, respectively. For group C, two peak values could be found which were larger than the maximum load of groups B and S, respectively. The properties of group C were better than those of groups B and S, except that the final displacement and energy consumption were located between those of groups B and S. Meanwhile, the linear equation in two unknowns have be found between groups B, S and C.

KEYWORDS: Beech dowel, self-tapping screw, composite dowel, shear performance.

INTRODUCTION

With the development of wood based engineering materials, especially laminated timber and cross-laminated timber (CLT), self-tapping screw (STS) connection was studied (Chen et al. 2019). Meanwhile, traditional wood dowels were also used to connect the CLT as a green and low carbon alternative (Hao et al. 2020, Bui et al. 2020, Li et al. 2020). Furthermore, a new wood dowel friction welding technology was another attempt (Bocquet et al. 2007, Bocquet et al. 2017, Girardon et al. 2014, Satoshi et al. 2017).

For the properties of components connected by STS, the lateral resistance performance of hex-head STS joint was better than that of wire nail joint except deforming ability (Sun et al. 2019). Considering the thread, the maximum load of screws with both double-threaded sections and fully threaded shanks were higher than those of single-threaded screws (Yeh et al. 2014). In the field of connecting the glulam, STS was often used with steel plate. Komatsu et al. (2019) studied the relationship between predicted nonlinear behaviors and observed ones. On the other hand, the influence of the angle of inclined screws was a research highlight. It was found that Tomasi model could be used to analyze the slip modulus of steel-wood joints when the angle between 45° to 90° (Lu et al. 2020). However, in the other study, an insertion angle of 30° had a larger stiffness and strength than a 45° angle (Mirdad et al. 2019, 2020a,b). Furthermore, if the length of STS was longer, the joint could increase the screwed in depth, then a higher shear properties obtained. Meanwhile, in this paper, Wang et al. (2020) proposed to use tapper washers to steady the inclined screws.

Based on the application of STS in the CLT. With the increased diameter and length, the shear strength could be improved (Sullivan et al. 2018, Dong et al. 2018). The stiffness and strength of specimens increased with the increase of angle too (Brown et al. 2020, Chang et al. 2019). Compared to the mortise-tenon connections in CLT, the STS connections failed before the damage of CLT, while the mortise-tenon connections did not failed (Lin et al. 2019). According to the Eurocode 5 and the study of Hossain et al. (2019), the group effect was 0.9n for all joints under static loading. In case of cyclic loading, a more pronounced group effect was observed that can be expressed as $n^{0.9}$ (n was the number of connected joints). Besides, self-tapping screws were used to connect the wooden parallel chord trusses. Fatal pull-out of self-tapping screws occurred by accompanying with bottom chord bending failure (Komatsu et al. 2018).

With the extending of using time, the cracks of the glulam and mortise-tenon joints occurred. Several researches have been studied the reinforcement by STS. The STS reinforcement could improve the capacity of glulam beam with cracks. This reinforcement method could prevent the development of cracks in the glulam beam during the bearing process (Petrycki et al. 2020, Zhang et al. 2019a,b). Johan et al. (2005) have found that the capacity of the reinforcement beams could improve 50% compared to the unreinforced beams. The compressive behavior increased obviously for the glulam specimens with self-tapping screws reinforcement. The length, number and the arrangement of the self-tapping screws had great influences on the failure modes and the load-carrying capacity (Tang et al. 2021). While in the reinforcement of mortise-tenon joints, the 5th percentile value of the capacity of beams with half-lap joint and round dovetail joint reinforced by self-tapping screws could reach

75.8-76.7% and 75.9-77.5% of that of the intact beams, respectively (Li et al. 2019). Song et al. (2018) studied the lateral performance of traditional heavy timber frames with mortise-tenon joints retrofitted using STS. The retrofitted frames exhibited smaller stiffness, larger deformability, higher damping ratio, and similar strength degradation from primary cycles to trailing cycles. In the research of Sun et al. (2018), it concluded that steel plates and STS are suitable for the strengthening of mortise-tenon joints, the strength or rigidity of which is obviously inadequate.

In this study, a new beech and self-tapping screw composite dowel was proposed. This composite dowel could have both of the features of STS and wood dowel. In the study of Zhu et al. 2017, 2018, 2019), the wood dowel could be broken by twisting. On the other hand, Liu et al. (2019) found that the twisting would be avoided when compressed wood was used, and the pullout resistance of compressed wooden dowel rotary friction welding could be increased. While in this paper, the twisting should also be avoided by using beech dowel instead of birch dowel, and the new composite dowel structural form. The shear performance of the component connected by the composite dowels was studied in this paper.

MATERIAL AND METHODS

Materials

Wood dowels, 12 mm in diameter and 70 mm in length, were fabricated from beech wood (*Zelkova schneideriana*, Crownhomes, Jiangsu, China). The dried density at 2% MC of the beech dowel was 703 $kg \cdot m^{-3}$. Self-tapping screws (Moregood, Shanghai, China), 5.2 mm in diameter and 70 mm in length, was covered by hot galvanizing. Spruce-pine-fir (SPF; Crownhomes, Jiangsu, China) slats with the dimensions of 89 mm (width, W) × 38 mm (thickness, T) × 300 mm (length, L) were used as substrates. The air dried density at 9.7% MC of the larch was 495 $kg \cdot m^{-3}$.

Specimen preparation

Group B (two beech dowels group): the wood substrates with the dimensions of 89 × 38 × 300 mm were pre-drilled with holes 10 mm in diameter and 70 mm in depth. Next, the wood dowels were welded into the pre-drilled holes in the substrates to create bonded joints at a high-speed rotation of 1500 rpm (Fig. 1b). Three specimens were prepared for each group.

Group S (two self-tapping screws group): the wood substrates with the dimensions of 89 × 38 × 300 mm were pre-drilled with holes 3 mm in diameter and 70 mm in depth. Next, the self-tapping screws were screwed into the pre-drilled holes in the substrates by electric hand drill. Three specimens were prepared for each group.

Group C (two composite dowels group): the wood dowels were pre-drilled with holes 3 mm in diameter and 70 mm in depth using a drilling machine. Then the self-tapping screws were screwed into the pre-drilled holes. Meanwhile, the wood substrates with the dimensions of 89 mm × 38 mm × 300 mm were pre-drilled with holes 10 mm in diameter and 70 mm in depth using a drilling machine. Next, the wood dowels were welded into the pre-drilled holes in the substrates to create bonded joints at a high-speed rotation of 1500 rpm (Fig. 1b). Three specimens were prepared for each group.

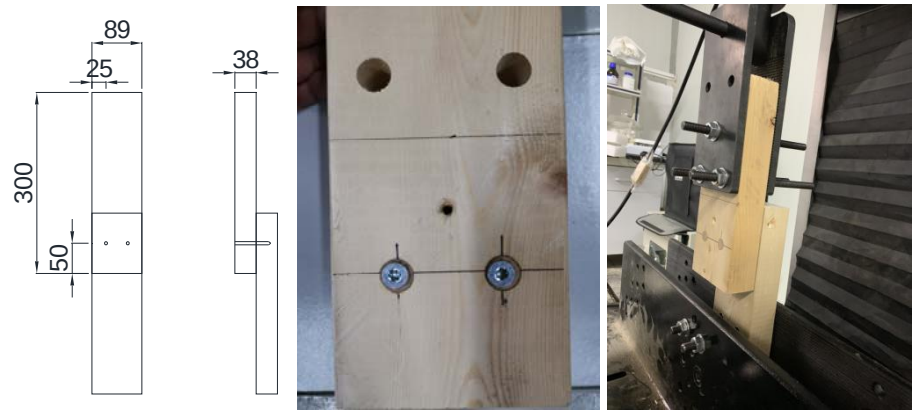

(a) *(b)* *(c)*

Fig. 1: The size of shear performance samples (a), samples of group C (b), and WDW-300E universal testing equipment.

Methods

Pullout resistance test

All the specimens were conditioned at 20°C and 60% relative humidity for 7 days before the tests were conducted. The pullout resistance of the specimens was tested using a universal testing machine (Fig. 1c, WDW-300E; Jinan Popwil, Jinan, China) at a speed of 5 $mm \cdot min^{-1}$.

Analysis method of characteristic value

All the force-displacement curves were obtained from the shear performance tests. Then each force-displacement curve was analyzed by analysis method of characteristic value (Fig. 2). According to this analysis, seven parameters which were maximum load (Pmax), ultimate load (Pu), yield load (Py), initial stiffness (Ki), ductility coefficient (μ), energy consumption (S) and final displacement (Du) could be calculated in Tabs. 1-3. From Fig. 2, six lines could be calculated and derived from the force-displacement curve. They were listed below:

I - the line connected by the points 0.1·Pmax and 0.4·Pmax;

II - the line connected by the points 0.4·Pmax and 0.9·Pmax;

III - move the line II to the tangent point of the force-displacement curve;

IV - draw a horizon line at the intersection of line I and III, extend the horizon line to the force-displacement curve, then the ordinate value was Py, the abscissa value was Dy;

V - the line connected by the point (0, 0) and (Dy, Py), the slope of the line was initial stiffness Ki;

VI - draw a line created the shadow area of figure which was equal to the area created by the force-displacement curve, X-ray, and the line X=Du, the ratio of Du and Dv was ductility coefficient μ.

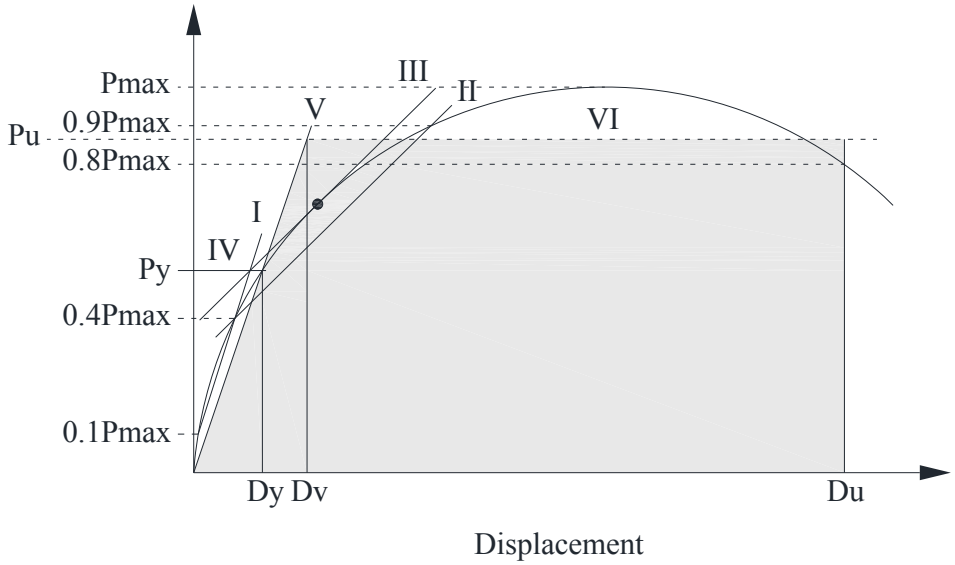

Fig. 2: Analysis method of characteristic value.

RESULTS AND DISCUSSION

The analysis of the curves and failure modes

All the curves of specimens were showed in Fig. 3. From Fig. 3a, all the maximum loads of group S were located at the displacement range of 20-25 mm. From Fig. 3b, three differences could be observed. First of all, the maximum loads of all the groups B were located at the displacement range 5-11 mm which were much smaller than those of the groups S. Second, when the loads were reached to the maximum value, they were decreased sharply to the zero. In the study of Hao et al. (2020) and Li et al. (2020), broken wood dowels were the main form of failure during the shear test. The similar phenomena were found in Fig. 5a, the broken beech dowels were the main failure modes of groups B. While from Fig. 4, the bending of self-tapping screws were the primary failure modes of group S. On the other hand, from Fig. 4d, the broken self-tapping screws after bending were the alternative failure modes of groups S. The failure modes of self-tapping screws were in accordance with Dong et al. (2018) and Lin et al. (2019). Third, the data diversity of groups B was much larger than that of groups S. The properties of self-tapping screws were similar to each other because the self-tapping screws were made from metal which was isotropic material. But beech wood was anisotropic material.

From Fig. 3c, one obvious difference could be found. Two peak values were observed. The first peak value was located at the range of 5-10 mm. And the second peak value was located at the range of 20-25 mm. The failure modes of groups C were showed in Fig. 5b. All the specimen showed the same failure mode. During all the test process, the bent of self-tapping screws and broken of beech dowels occurred simultaneously. On the other hand, combined with the two peak values, the beech dowels were broken when the curves reached to the first peak value. The self-tapping screws were bent to the limit state when the curves reached to the second peak value.

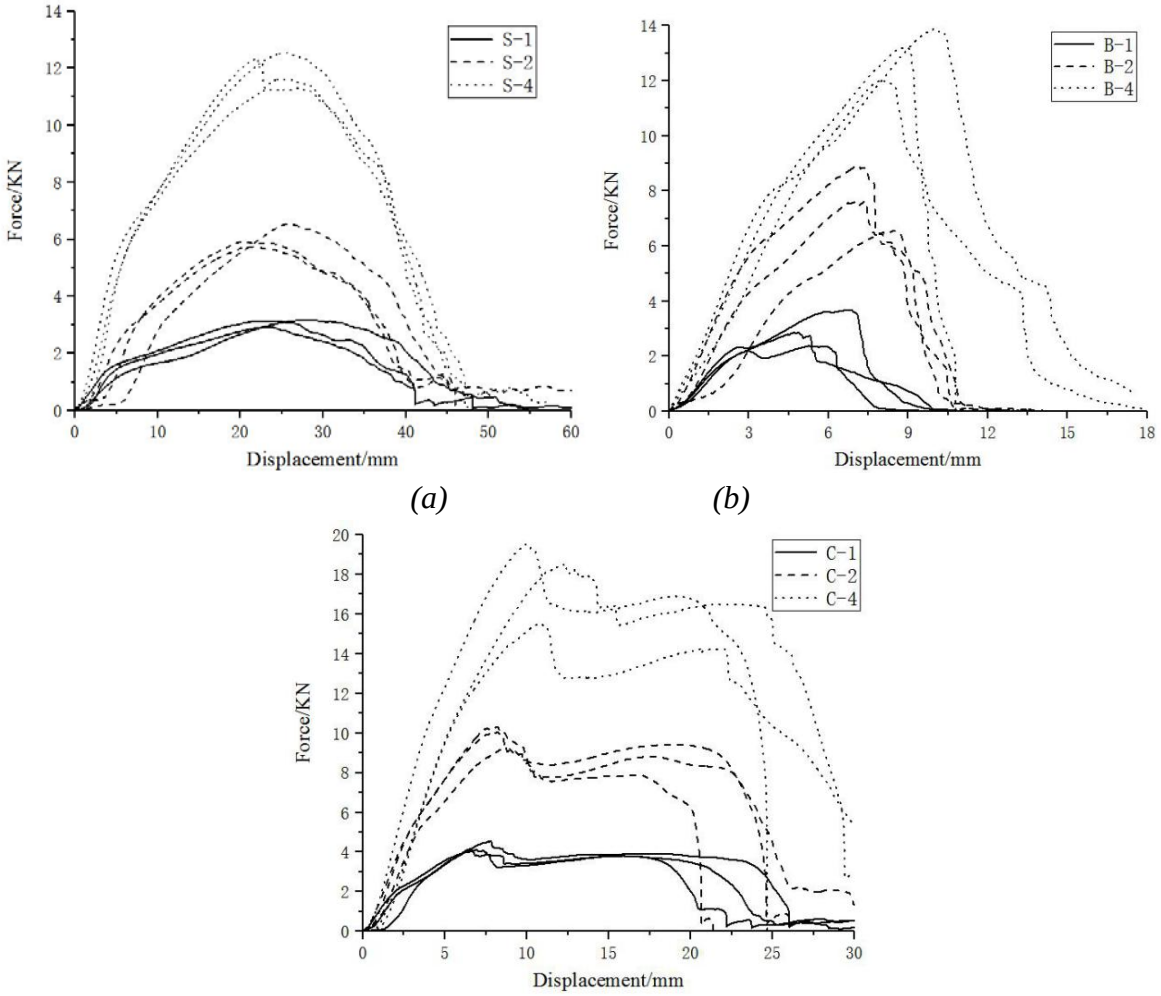

(a) *(b)*

(c)

Fig. 3: Force displacement curves of group S (a), B (b), and C (c).

(a) *(b)* *(c)* *(d)*

Fig. 4: Failure mode of group S-1 (a), S-2 (b), S-4-1 (c), and S-4-3 (d).

(a) *(b)*

Fig. 5: Failure mode of group B (a), and C (b).

Tab. 1: Shear performance of group S.

Parameters	S-1			S-2			S-4		
	S-1-1	S-1-2	S-1-3	S-2-1	S-2-2	S-2-3	S-4-1	S-4-2	S-4-3
Maximum load (kN)	2.910	3.150	3.130	5.910	5.740	6.540	11.300	12.350	12.520
	3.063(0.133)[1]			6.063(0.421)			12.057(0.661)		
Yield load (kN)	1.340	1.316	1.430	3.010	2.555	3.023	5.330	5.065	5.660
	1.362(0.060)			2.863(0.267)			5.532(0.298)		
Ultimate load (kN)	2.420	2.627	2.640	5.216	5.000	5.550	9.865	10.360	10.895
	2.562(0.123)			5.255(0.277)			10.373(0.515)		
Initial stiffness ($kN \cdot mm^{-1}$)	0.294	0.219	0.366	0.404	0.457	0.288	0.903	1.099	0.897
	0.293(0.074)			0.383(0.086)			0.966(0.115)		
Ductility coefficient	3.761	3.134	4.283	2.467	2.920	1.788	3.189	3.446	2.798
	3.726(0.575)			2.392(0.570)			3.144(0.326)		
Final displacement (mm)	30.948	37.529	30.908	31.838	31.912	34.503	34.854	32.490	33.973
	33.128(3.811)			32.751(1.518)			33.772(1.195)		
Energy consumption ($kN \cdot mm$)	64.938	82.850	72.053	132.41	132.26	137.96	289.97	287.75	304.04
	73.280(9.019)			134.21(3.248)			293.92(8.834)		

[1]Values in parentheses are the standard deviation.

Tab. 2: Shear performance of group B.

Parameters	B-1			B-2			B-4		
	B-1-1	B-1-2	B-1-3	B-2-1	B-2-2	B-2-3	B-4-1	B-4-2	B-4-3
Maximum load (kN)	3.690	2.380	2.860	6.560	7.610	8.900	13.200	12.050	13.900
	2.977(0.663)			7.690(1.172)			13.050(0.934)		
Yield load (kN)	1.945	2.052	1.647	4.440	3.690	4.910	7.676	7.322	5.612
	1.881(0.210)			4.347(0.615)			6.870(1.104)		
Ultimate load (kN)	3.068	2.128	2.478	5.580	6.343	7.630	11.620	10.253	12.533
	2.558(0.475)			6.518(1.036)			11.469(1.148)		
Initial stiffness ($kN \cdot mm^{-1}$)	0.982	0.804	0.873	0.946	1.477	1.946	1.953	2.185	1.634
	0.886(0.090)			1.456(0.500)			1.924(0.277)		
Ductility coefficient	2.300	2.378	1.892	1.543	1.865	1.975	1.562	1.895	1.420
	2.190(0.261)			1.794(0.225)			1.626(0.244)		
Final displacement (mm)	7.185	6.292	5.370	9.103	8.008	7.745	9.295	8.895	10.886
	6.282(0.908)			8.285(0.720)			9.692(1.053)		
Energy consumption ($kN \cdot mm$)	17.240	10.570	9.792	33.366	37.175	44.128	73.415	67.139	88.370
	12.534(4.094)			38.223(5.457)			76.308(10.904)		

Tab. 3: Shear performance of group C.

Parameters	C-1			C-2			C-4		
	C-1-1	C-1-2	C-1-3	C-2-1	C-2-2	C-2-3	C-4-1	C-4-2	C-4-3
Maximum load (kN)	4.030	4.540	4.120	10.040	9.280	10.300	19.520	18.510	15.500
	4.230(0.272)			9.873(0.530)			17.843(2.091)		
Yield load (kN)	1.862	1.890	2.400	4.634	4.766	4.776	9.640	9.404	8.832
	2.051(0.303)			4.725(0.079)			9.292(0.415)		
Ultimate load (kN)	3.576	3.747	3.601	8.457	7.832	8.967	16.613	16.232	13.326
	3.641(0.092)			8.419(0.568)			15.390(1.798)		
Initial stiffness (kN.mm-1)	1.055	0.881	0.695	1.805	1.502	1.775	2.625	1.917	1.882
	0.877(0.180)			1.694(0.167)			2.141(0.419)		
Ductility coefficient	6.214	4.198	4.614	4.796	3.455	4.446	3.373	2.957	3.252
	5.009(1.064)			4.232(0.696)			3.194(0.214)		
Final displacement (mm)	21.061	17.847	23.911	22.477	18.019	22.464	21.345	25.039	23.028
	20.940(3.034)			20.987(2.570)			23.137(1.849)		
Energy consumption (kN·mm)	69.254	58.908	76.766	170.281	120.702	178.779	302.040	337.707	259.691
	68.309(8.966)			156.587(31.367)			299.813(39.056)		

The difference of parameters among group B, S, and C

From Tabs. 1-3 and Fig. 6a, the maximum load increased with the number for all the groups which was illustrated above (Liu et al. 2015, Hossain et al. 2019). The maximum loads of groups C were higher than those of groups B and S individually, but lower than the sum of groups B and S. On the other hand, the second peak values were existed in groups C beside the maximum loads. The sum of the two peak values was much higher than the sum of the group B and S.

From Fig. 6b, the initial stiffness of groups S was the lowest. While the initial stiffness of groups B was a little lower than that of groups C. From the curves of Fig. 3, in the displacement range of 0-5 mm, the curve shape of groups C was similar to that of groups B which increased sharply. The curve shape of groups S increased slowly. Based on these phenomena, the initial stiffness of groups S was much lower than that of the other two groups (Dong et al. 2015, Xiong et al. 2011). With the increased connector number, the initial stiffness showed the increasing trend.

From Fig. 6c, the final displacement of groups S was the largest. On the contrast, the final displacement of groups B showed the lowest value. While the final displacement of groups C was situated between the groups B and S. For the same groups, the final displacement of different connector number did not show obvious difference. From Fig. 6d, the ductility coefficient of groups B was the lowest because the final displacement of groups B was the lowest. For the groups C, the ductility coefficient was the highest, because the final displacement of them was higher than that of groups B, the initial stiffness of groups C was higher than that of groups S. On the other hand, the initial stiffness increased with the connector number (Liu et al. 2015), while the final displacement did not showed the obvious change with the connector number. Based on this, the ductility coefficient showed the downward trend with the connector number. From Fig. 6e, the changing trend of energy consumption was similar to that of maximum load in Fig. 6a.

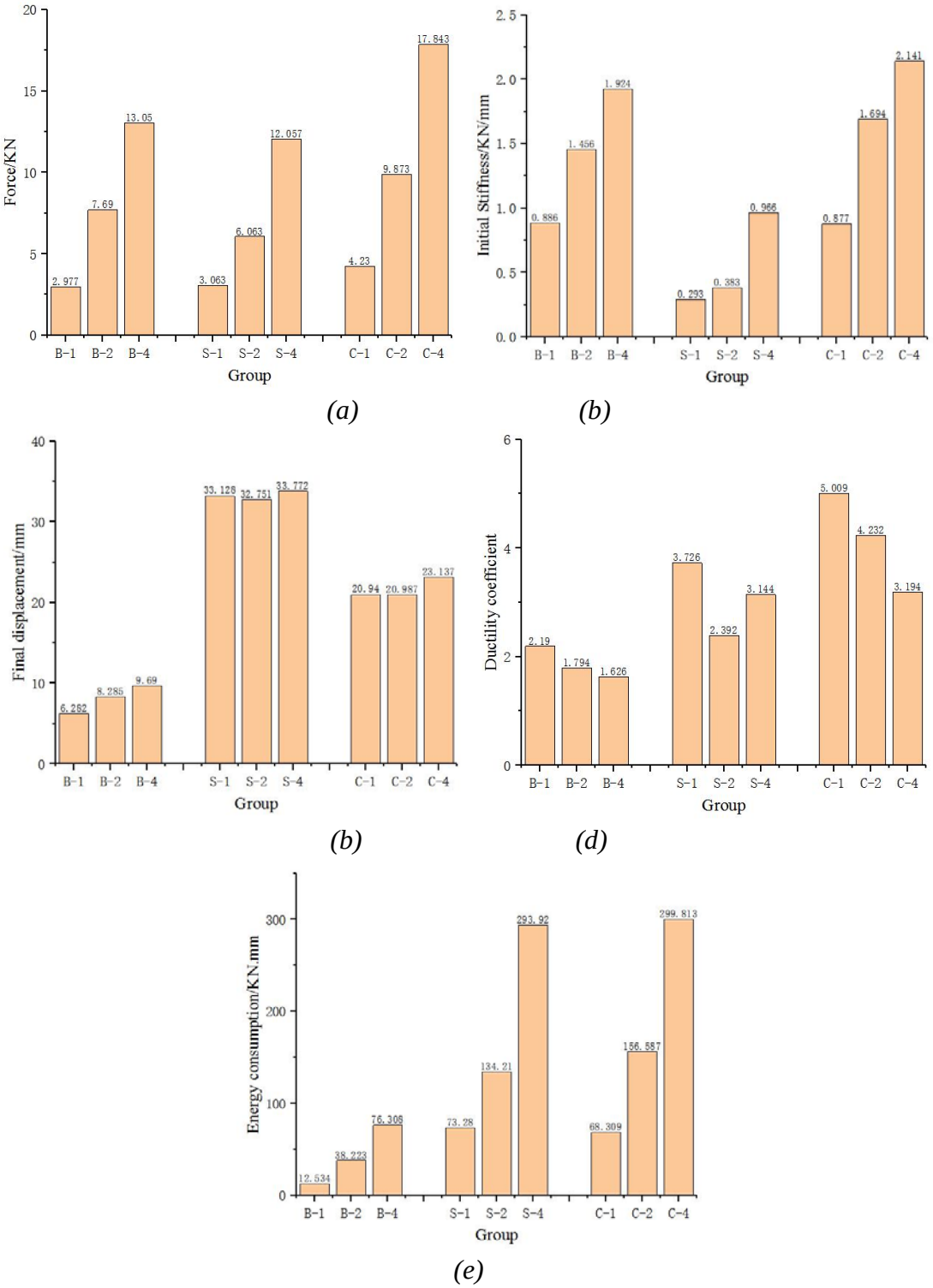

Fig. 6: The difference of maximum load (a), initial stiffness (b), final displacement (c), ductility coefficient (d), and energy consumption (e) between group B, S, and C.

The relationship between group B, S, and C

The relationship between groups B, S, and C was studied below (Xue et al. 2020). The value of group B-1, and B-2 was set as *x*, the value of group S-1, and S-2 was set as *y*, and the value of group C-1 and C-2 was set as *z*. Then the linear equation in two unknowns could be

observed. And then using the formulas, the calculated values of groups C-3 could be found in Tab. 4. On the other hand, the errors between calculated values and testing values could also be found in Tab. 4. The errors of the parameters of yield load, initial stiffness, and ductility coefficient were higher than 10%. So this evaluation method could not be used in these three parameters reasonably. However, in the other five parameters, this analysis method could be a good choice, especially the maximum load, the second peak value, and ultimate load. According to this study, the maximum load, the second peak value, and ultimate load of groups C could be calculated accurately. In the future study, more evidence of the relation between groups B, S, and C could be explored:

$$\text{Maximum load: } z = 0.57x + 0.835y \quad (1)$$

$$\text{The second maximum load: } z = 0.707x + 0.575y \quad (2)$$

$$\text{Yield load: } z = 0.052x + 1.053y \quad (3)$$

$$\text{Ultimate load: } z = 0.674x + 0.748y \quad (4)$$

$$\text{Initial stiffness: } z = -2.566x + 1.839y \quad (5)$$

$$\text{Ductility coefficient: } z = -0.195x + 2.619y \quad (6)$$

$$\text{Final displacement: } z = 0.606x + 0.138y \quad (7)$$

$$\text{Energy consumption: } z = 0.579x + 2.062y \quad (8)$$

Tab. 4: The difference between calculated value and test value.

Parameters	Maximum load	The second maximum load	Yield load	Ultimate load
Calculated value	17.762	16.026	7.520	15.574
Test value	17.843	15.877	9.292	15.390
Error (%)	0.45	0.94	19.07	1.19
Parameters	Initial stiffness	Ductility coefficient	Final displacement	Energy consumption
Calculated value	1.058	3.645	21.799	327.666
Test value	2.141	3.194	23.137	299.813
Error (%)	50.57	14.13	5.78	9.29

CONCLUSIONS

(1) The maximum load, yield load, ultimate load, and initial stiffness of groups B were better than those of groups S. The ductility coefficient, final displacement, and energy consumption of groups B were lower than those of groups S. The main failure mode of groups B was the broken beech dowel. While for groups S, the bent self-tapping screw was the main failure mode. *(2)* The maximum load, yield load, ultimate load, initial stiffness, and ductility coefficient of groups C were better than those of groups B, and S. Two peak values could be found in groups C. The first and second peak values were larger than those of groups B and S, respectively. The final displacement and energy consumption of groups C were located between those of groups B and S. *(3)* The linear equation in two unknowns have be found between groups B, S and C. It could be used to calculate the maximum load, the second peak value, and ultimate load of groups C, when the parameters of groups B and S were obtained.

ACKNOWLEDGMENTS

The authors are grateful for the support of the National Natural Science Foundation of China (Grant No. 31901252), the Natural Science Foundation of Jiangsu Province, China (Grant No. BK20180276), Jiangsu Planned Projects for Postdoctoral Research Funds (Grant No. 2020Z075), the Science and Technology Program of Jiangsu Housing and Construction Department (Grant No. 2018ZD118, No. 2020ZD039, No. 2020ZD043 and No. 2021ZD026), Qing Lan Project of Jiangsu, the Yangzhou Science and Technology Project (Grant No. SGH2020010040), and the Natural Science Foundation of the Jiangsu Higher Education Institutions of China (Grant No. 18KJB220012).

REFERENCES

1. Bocquet, J.F., Pizzi, A., and Despres, A., Mansouri, H.R., Resch, L., Michel, D., Letort, F., 2017: Wood joints and laminated wood beams assembled by mechanically-welded wood dowels. Journal of Adhesion Science and Technology 21(3/4): 301- 317.
2. Bocquet, J.F., Pizzi, A., Resch, L., 2007: Full-scale industrial wood floor assembly and structures by welded-through dowels. European Journal of Wood and Wood Products 65(2): 149-155.
3. Brown, J.R., Li, M.H., Tannert, T., Moroder, D., 2020: Experimental study on orthogonal joints in cross-laminated timber with self-tapping screws installed with mixed angles. Engineering Structures 228(1): 1-14.
4. Bui, T.A., Oudjene, M., Lardeur, P., Khelifa, M., Rogaume, Y., 2020: Towards experimental and numerical assessment of the vibrational serviceability. Engineering Structures 216: 1-10.
5. Chang, C., Fang, Y.F., Liu, Y.F., Que, Z.L., 2019: Study on pull-out performance of tilted self-tapping screw in cross-laminated timber. Architecture Technology 50(4): 416-418.
6. Chen, H., Liu, Z.B., Li, S.Z., He, X.P., 2019: A summary of research on the connection performance of new self-tapping screws in wood structures. Shanxi Architecture 45(1): 34-35.
7. Dong, W.B., Gao, Y., Yu, Z.M., Yuan, T.G., 2015: Experimental research on MIDPLY shear wall nail joints of light wood structures. Building Structure 45(6): 54-57.
8. Dong, W.Q., Yao, Y., Song, H., Qi, Y.Y., Ren, H.Q., Wang, Z.Q., 2018: Shear strength of cross-laminated timber connected with self-tapping screws. China Wood Industry 32(5): 1-5.
9. Girardon, S., Barthram, C., Resch, L., Bocquet, J.F., Triboulot, P., 2014: Determination of shearing stiffness parameters to design multi-layer spruce beams using welding-through wood dowels. European Journal of Wood and Wood Products 72(6): 721-733.
10. Hao, J.X., Xu, L., Wu, X.F., Li, X.J., 2020: Analysis and modeling of the dowel connection in wood T type joint for optimal performance. Composite Structures 253:1-11.
11. Hossain, A., Popovski, M., Tannert, T., 2019: Group effects for shear connections with self-tapping screws in CLT. Journal of Structural Engineering 145(8): 1-9.

12. Johan, J., 2005: Load carrying capacity of curved glulam beams reinforced with self-tapping screws. Holz. als Roh- und Werkstoff 63: 342-346.
13. Komatsu, K., Teng, Q.C., Li, Z.R., Zhang, X.L., Que, Z.L., 2018: Experimental and numerical analyses on nonlinear behaviour of wooden parallel chord trusses composed of self-tapping screws. Journal of Wood Science 64(2): 776-793.
14. Komatsu, K., Teng Q.C., Li, Z.R., Zhang, X.L., Que, Z.L., 2019: Experimental and analytical investigation on the nonlinear behaviors of glulam moment-resisting joints composed of inclined self-tapping screws with steel side plates. Advances in Structural Engineering 22(15): 3190-3206.
15. Li, H.M., Lam, F., Qiu, H.X., 2019: Comparison of glulam beam-to-beam connections with round dovetail and half-lap joints reinforced with self-tapping screws. Construction and Building Materials 227: 1-11.
16. Li, Q., Song, H., Wang, Z.Q., 2020: Bending performance of timber composite beam fastened with bamboo/wood dowels. Journal of Northwest Forestry University 35(2): 218-222.
17. Lin, Q. Y., Wen, C. S., Diao, Y., Yan, L. R., Gao, Y., 2019: Mechanical properties of CLT shear connections between self-tapping screws and mortise tenons. Journal of Beijing Forestry University 41(11): 146-154.
18. Liu, K., 2019: Study on pullout resistance of compressed wooden dowel rotary friction welding. Master's thesis. Pp 34-48, Dalian University of Technology, China.
19. Liu, H.F., He, M.J., 2015: Effects of self-tapping screw on performance of glulam beam-to-column connections. Journal of Building Structures 7: 148-156.
20. Lu, X.R., Teng, Q.C., Li, Z.R., Zhang, X.L., Wang, X.M., Komatsu, K., Que, Z.L., 2020: Study on shear property of spruce glulam and steel plate connected with inclined screw. Journal of Forestry Engineering 5(3): 48-53.
21. Mirdad, M.A.H., Chui, Y.H., 2019: Load-slip performance of mass timber panel-concrete (MTPC) composite connection with Self-tapping screws and insulation layer. Construction and Building Materials 213: 696-708.
22. Mirdad, M.A.H., Chui, Y.H., 2020: Stiffness prediction of mass timber panel-concrete (MTPC) composite connection with inclined screws and a gap. Engineering Structures 207: 1-11.
23. Mirdad, M.A.H., Chui, Y.H., 2020: Strength prediction of mass-timber panel concrete-composite connection with inclined screws and a gap. Journal of Structural Engineering 146(8): 1-13.
24. Petrycki, A., Salem, S., 2020: Structural integrity of bolted glulam frame connections reinforced with self-tapping screws in a column removal scenario. Journal of Structural Engineering 146(10): 1-13.
25. Satoshi, F., Keita, O., Masaki, N., Yamasaki, M., Sasaki, Y., 2017: Shear properties of metal-free wooden load-bearing walls using plywood jointed with a combination of adhesive tape and wood dowels. European Journal of Wood and Wood Products 75(3): 429-437.

26. Song, X.B., Li, K., Crayssac, E., Wu, Y.J., 2018: Lateral performance of traditional heavy timber frames with mortise-tenon joints retrofitted using self-tapping screws. Journal of Structural Engineering 144(10): 1-10.
27. Sullivan, K., Miller, T.H., Gupta, R., 2018: Behavior of cross-laminated timber diaphragm connections with self-tapping screws. Composite Structures 168: 505-524.
28. Sun, Y.H., Jiang Z.H., Zhang X.B., Sun, Z.J., Liu, H.R., 2019: Behavior of glued laminated bamboo and bamboo-oriented strand board sheathing-to-framing connections. European Journal of Wood and Wood Products 77: 1189-1199.
29. Sun, Z.Y., Cheng, X.W., Lu, W.D., 2018: Experimental study on seismic performance of damaged straight mortise-tenon joints of ancient timber buildings strengthened with steel plates and self-tapping screws. Structural Engineers 34(5): 106-112.
30. Tang, L.Q., Xu, W., Yang, H.F., Tan, G.H., Chen, Y., 2021: Compressive strength tests perpendicular to the grain of glulam reinforced with self-tapping screws. Journal of Nanjing Technology University (Natural Science Edition) 43(1): 94-100.
31. Wang, C.L., Lyu, J.F., Zhao, J., Yang, H.F., 2020: Experimental investigation of the shear characteristics of steel-to-timber composite joints with inclined self-tapping screws. Engineering Structures 215(15): 1-17.
32. Xiong, H.B., Pan, Z.F., Kang, J.H., Hua, M.X., 2011: Test study on behavior of stud-to-sheathing nail joints under monotonic load in light wood frame constructions. Structural Engineers 6: 106-112.
33. Xue, Y.Y., Zhu, X.D., 2020: Study on the relationship between the MOE of lumbers and nail-laminated timbers. China Forest Products Industry 5:16-20.
34. Yeh, M.C., Lin, Y.L., Huang, G.P., 2014: Investigation of the structural performance of glulam beam connections using self-tapping screws. Journal of Wood Science 60: 39-48.
35. Zhang, C., Guo, H.B., Jung, K., Harris, R., Chang, W.S., 2019: Screw reinforcement on dowel-type moment-resisting connections with cracks. Construction and Building Materials 215: 59-72.
36. Zhang, C., Guo, H. B., Jung, K., Harris, R., Chang, W. S., 2019: Using self-tapping screw to reinforce dowel-type connection in a timber portal frame. Engineering Structures 178: 656-664.
37. Zhu, X.D., Gao, Y., Yi, S., Ni, C., Zhang, J., Luo, X., 2017: Mechanics and pyrolysis analyses of rotation welding with pretreated wood dowels. Journal of Wood Science 63(3): 216-224.
38. Zhu, X.D., Xue, Y.Y., Zhang, S.J., Zhang, J., Shen, J., Yi, S.L., Gao, Y., 2018: Mechanics and crystallinity/thermogravimetric investigation into the influence of the welding time and $CuCl_2$ on wood dowel welding. BioResources 13(1): 1329-1347.
39. Zhu, X.D., Xue, Y.Y., Shen, J., Zhang, S.J., 2019: Withdrawal strength of welded dowel joints made of birch and larch wood. Wood Research 64(5): 921-934.

XUDONG ZHU[1,2]
[1]NANJING FORESTRY UNIVERSITY
JIANGSU, 210037
[2]YANGZHOU POLYTECHNIC INSTITUTE
[3]YANGZHOU UNIVERSITY
JIANGSU, 225100
CHINA

YINGYING XUE, XUEWEN ZHANG, PENGFEI QI, JIE SHEN
YANGZHOU POLYTECHNIC INSTITUTE
JIANGSU, 225100
CHINA

CHANGTONG MEI*
NANJING FORESTRY UNIVERSITY
JAINGSU, 210037
CHINA
*Corresponding author: mei@njfu.edu.cn